# X-ray-absorption studies of zirconia polymorphs. III. Static distortion and thermal distortion

Ping Li and I-Wei Chen
*Department of Materials Science and Engineering, University of Michigan, Ann Arbor, Michigan 48109-2136*

James E. Penner-Hahn
*Department of Chemistry, University of Michigan, Ann Arbor, Michigan 48109-1055*
(Received 10 March 1993; revised manuscript received 28 May 1993)

Static and dynamic Debye-Waller factors for the Zr(Y)-O shell and the Zr(Y)-Zr(Y) shell have been determined for four zirconia polymorphs from 10 K to room temperature. The apparent Einstein frequencies for cation-O vibrations and the Debye frequencies for cation-cation vibrations have also been obtained from the analysis. The higher phase stability and the stabilizing effect of Y dopants are manifest in the higher apparent vibrational frequencies. For tetragonal zirconia these frequencies correlate well with Raman data, and for cubic zirconia the Y-O frequency coincides with the unique Raman frequency for fluorite-structure oxides. Similar bonding in monoclinic and cubic zirconia yields similar vibrational frequencies, while a larger bond distance generally leads to a lower frequency. Comparison of the Debye-Waller factors obtained from extended x-ray-absorption fine structure and from neutron diffraction has also revealed the different extent of atom-atom correlation in atomic thermal motion for different bonding.

## I. INTRODUCTION

The amplitude observed in an extended x-ray-absorption fine structure (EXAFS) spectrum is damped due to disorder in the scattering shell. This sensitivity to disorder can be used to obtain information which may not be available from other techniques. The disorder effects in EXAFS can be described in terms of a Debye-Waller factor ($\sigma^2$), which is the mean-square deviation in the average distance between absorbing atom and scattering atom. Both thermal distortions ($\sigma^2_{vib}$) caused by thermal vibration and static distortions ($\sigma^2_{stat}$) due to structural variation or chemical differences within a shell contribute to the observed $\sigma^2$. These two contributions can be separated with the aid of appropriate models if the full temperature dependence of the EXAFS amplitude is known.[1,2]

Thermal distortion is related to the local, projected density of vibrational modes.[3] It is thus reasonable to use $\sigma^2_{vib}$ to determine an apparent vibrational frequency. The vibrational frequency determined in this way is an average value of all relevant vibrational modes. It can be used as a qualitative measure of bond strength for closely related systems. The static distortion provides information about the deviation of the local configurations from their mean (which quite often corresponds to the ideal crystalline counterparts). In addition, as we demonstrate in this work, a careful comparison of the Debye-Waller factors in EXAFS and diffraction can lead to information on the atom-atom correlation in atomic motion.

In the preceding papers (referred to as I and II hereafter),[4,5] we have used x-ray-absorption spectroscopy to determine the local Zr structure in four zirconia polymorphs (monoclinic, orthorhombic, tetragonal, and cubic zirconia). In addition, the local structure of the Y solute has also been determined. Valuable knowledge of the characteristic local structures of Y and Zr, the type and distortion of their oxygen polyhedra, and the local and longer-range cation network configurations have been obtained from such a study. In the present work, we have measured the temperature dependence of the Zr and Y EXAFS. The data are analyzed using simple vibrational models and compared with Raman spectra and diffraction data in order to gain further structural insight into the static and thermal stability of various zirconia polymorphs.

## II. EXPERIMENTAL PROCEDURE

### A. Materials

Pure monoclinic ($m$-$ZrO_2$) and orthorhombic ($o$-$ZrO_2$) zirconia, 3 mol% $Y_2O_3$-stabilized tetragonal zirconia ($t$-$ZrO_2$), and 20 mol% $Y_2O_3$-stabilized cubic zirconia ($c$-$ZrO_2$) were investigated in this study. These materials are identical to the ones reported in I. Powders of yttria-stabilized tetragonal and cubic zirconia were prepared by a coprecipitation method and calcined at 1300 °C for 4 h, usually sufficient to fully form a $Y_2O_3$-$ZrO_2$ solid solution. The undoped monoclinic zirconia powder was synthesized following a similar procedure but calcined at 1200 °C. The orthorhombic zirconia powder was prepared at 600 °C and 6 GPa before quenching to ambient condition.[6,7] Phase identification and characteristic x-ray-diffraction (XRD) patterns of these four zirconia powders have been described elsewhere (Fig. 3 in I).[4]

### B. X-ray-absorption measurements

X-ray-absorption spectroscopy (XAS) measurements were performed at the Zr $K$ edge for $m$-$ZrO_2$ and $o$-$ZrO_2$,

 

and at both the Zr $K$ edge and the Y $K$ edge for $t$-$ZrO_2$ and $c$-$ZrO_2$. The temperatures used were 10, 100, 200, and 300 K. All of the data were collected in transmission mode on Beamline 7-3 at the Stanford Synchrotron Radiation Laboratory. Energy selection was accomplished by using a double-crystal monochromator with Si(220) crystals. The calibration was determined by assigning the highest inflection point of the Zr $K$ edge in $m$-$ZrO_2$ as 17 998 eV and of the Y $K$ edge in $Y_2O_3$ as 17 038 eV. These procedures are the same as those in I and II.

The EXAFS data analysis also followed the same procedures described in I and II using theoretical amplitude and phase-shift functions calculated from the FEFF program.[8] Since Zr and Y have very similar scattering behavior and atomic mass, it is appropriate to treat the next-nearest neighbor (NNN) as Zr in all cases. The Debye-Waller factor (as a fitting parameter) of each shell thus obtained is written as the sum of two contributions:

$$\sigma^2=\sigma^2_{\text{stat}}+\sigma^2_{\text{vib}} . \tag{1}$$

The former is temperature independent and corresponds to the dispersion of bond lengths without vibration. The latter is due to thermal vibration and is thus related to the vibrational spectrum. Appropriate models are then used to separate these contributions.

### C. Vibration analysis

There are two approximations for describing the vibrational contributions.[9,10] For the first shell data in an oxide, the cation-oxygen vibration can be approximately regarded as the optical mode of the phonon spectrum. In this case, an Einstein model is appropriate because the vibrational frequency of the diatomic optical mode is typically high and relatively wavelength independent. For the second shell data, the cation-cation vibrations (Zr-Zr or Y-Zr) involved are clearly not optical modes. Since longer-wavelength acoustic modes of the cation network are probably more important in this case, we have adopted the Debye model with a distribution of vibrational frequencies to analyze the second-shell data.

The vibrational contribution, based on an Einstein model, can be written as

$$\sigma^2_{\text{vib}}=\frac{h}{8\pi^2\mu\nu}\coth\left[\frac{h\nu}{2kT}\right] . \tag{2}$$

For a Debye model, it is

$$\sigma^2_{\text{vib}}=\frac{3k^2T^2}{8\pi^2Mh\nu^2}\int_0^{h\nu/kT}\left[\frac{1}{e^x-1}+\frac{1}{2}\right]x\,dx . \tag{3}$$

In the above, $\mu$ is the reduced mass of the cation-oxygen pair, $M$ is the cation mass, $T$ is the temperature, $k$ is Boltzmann's constant, and $h$ is Planck's constant. The frequency $\nu$ is the so-called Einstein frequency for the optical mode in Eq. (2) or the Debye frequency, which is the maximum vibrational frequency of the acoustic mode in Eq. (3). Both equations give nonzero $\sigma^2_{\text{vib}}$ values at 0 K, corresponding to zero-point motion. Combining Eqs. (1) and (2), we can fit the cation-oxygen data to determine the Einstein vibrational frequency and the static distortion. Likewise, from Eqs. (1) and (3), the Debye frequency and the static distortion can be obtained for the cation-cation shell.

## III. RESULTS

### A. Temperature dependence of the EXAFS spectra

The Fourier transforms (FT's) of the Zr EXAFS for the four polymorphs obtained at different temperatures are shown in Figs. 1–4. The characteristic spectra of the different zirconia phases described in I are observed here at all temperatures. The characteristic features of each polymorph, in terms of the peak positions and shapes, remain unchanged throughout the temperature range, implying that no phase transformation occurred during cooling down to 10 K, even though some of the phases ($o$-$ZrO_2$ and $t$-$ZrO_2$) were only metastable. The main effect of the temperature is on the amplitude. The amplitude decreases slightly from 10 to 100 K and more dramatically above 100 K. The decrease is relatively more drastic for the outer shells than for the inner shells. At room temperature, the outer peaks have diminished so much that they are no longer detectable in most cases.

One of our previous observations was the unusual strength of the second peak in the tetragonal phase at 10 K.[4] This is evident in Fig. 3 where the height of the second peak at 10 K is much higher than that of the other three phases (Figs. 1, 2, and 4) at the same temperature. (Note the difference in scale for Figs. 1–4.) At higher temperatures, this contrast is not evident. At 300 K, all of the second peaks have a peak height of approximately 20, with the exception of cubic phase.

EXAFS spectra at the Y $K$ edge for $t$-$ZrO_2$ and $c$-$ZrO_2$ were also obtained at these temperatures. Their corresponding FT's are given in Figs. 5 and 6. As for the Zr data, the amplitude decreases with increasing temperature and the decrease is more pronounced above 100 K. Also note the very high amplitude of the second peak in $t$-$ZrO_2$ at 10 K which drops to a more modest value at 300 K. These features are all similar to those found for Zr, and as with Zr, the outer peaks are nearly unresolvable at room temperature.

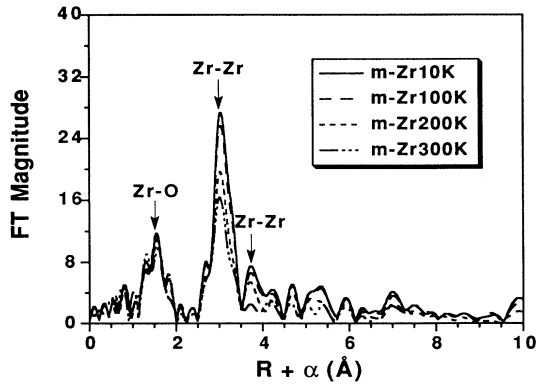


FIG. 1. Temperature dependence of Fourier transform of Zr EXAFS for $m$-$ZrO_2$.

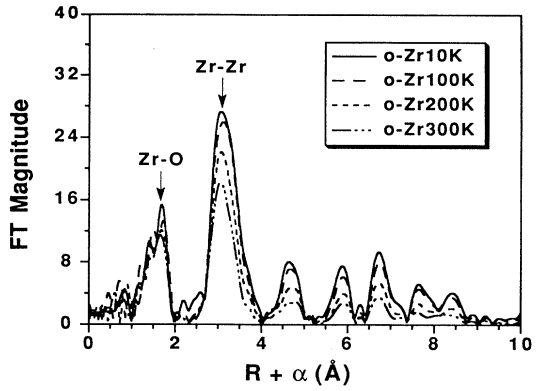


FIG. 2. Temperature dependence of Fourier transform of Zr EXAFS for $o$-$ZrO_2$.

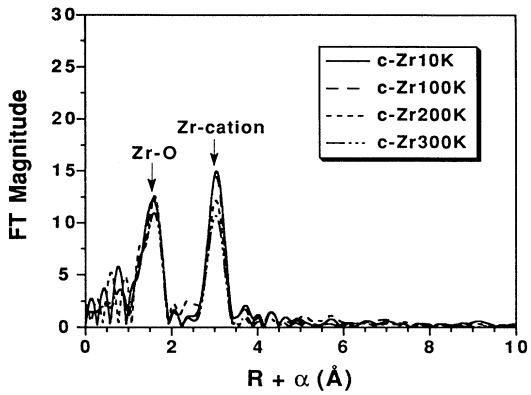


FIG. 4. Temperature dependence of Fourier transform of Zr EXAFS for Y-stabilized $c$-$ZrO_2$.

Curve fitting has been used for quantitative analysis which gives characteristic structural parameters. They are temperature independent within the accuracy of the EXAFS analysis. These structural parameters have been discussed in detail in I and II. The main new information is now contained in the temperature dependence of the Debye-Waller factor, which increases monotonically with increasing temperature, as shown in Figs. 7 and 8, and accounts for the decreased amplitude in the FT. Quantitative analysis using an Einstein model (in Fig. 7) for cation-oxygen shell and a Debye model (in Fig. 8) for cation-cation shells gives $\sigma^2_{\text{stat}}$ and reduced apparent frequency $\bar{\nu}$ ($\bar{\nu}=\nu/c$, where $c$ is the velocity of light) tabulated in Table I.

### B. Static distortion

#### 1. *Cation-oxygen shells*

As described in I, $m$-$ZrO_2$, $o$-$ZrO_2$, and $c$-$ZrO_2$ all have similar seven-coordinate Zr-O bonding. The average Zr-O bond lengths determined from EXAFS are in good agreement with the crystallographic data. As shown in Table I, the Zr-O $\sigma^2_{\text{stat}}$ is the largest for $m$-$ZrO_2$ (0.0070 Å$^2$), followed by $c$-$ZrO_2$ (0.0045 Å$^2$), and the smallest for $o$-$ZrO_2$ (0.0031 Å$^2$). The bond dispersions calculated from crystallographic data for $m$-$ZrO_2$ (0.0071 Å$^2$) and $o$-$ZrO_2$ (0.0030 Å$^2$) are in excellent agreement with the EXAFS results. This is most satisfying since our fitting procedure is based on *ab initio* parameters and contains no adjustable empirical parameter other than a single $E_0$ which was fixed for all data analysis. No comparison was possible for $c$-$ZrO_2$ due to the lack of definitive crystallographic data for the oxygen positions in this alloy system. However, we are confident that the static dispersion of the Zr-O bond length in $c$-$ZrO_2$ is intermediate between those in $m$-$ZrO_2$ and $o$-$ZrO_2$.

As shown by the FT data in Fig. 9 and discussed in I and II, the Zr-O shell in the tetragonal structure is split into two subshells. This is illustrated in the inset of Fig. 9 by the two distinct oxygen positions, $O_I$ and $O_{II}$. The two-shell structure is clearly resolved at 10 K, but becomes less resolved at higher temperatures. Fitting based on an Einstein model gives a very small static distortion for Zr-$O_I$ (0.0005 Å$^2$) and a much larger value for Zr-$O_{II}$ (0.0049 Å$^2$). Such information is unique to EXAFS. In the diffraction studies, a periodic model such as the one in the inset of Fig. 9 must be assumed. By symmetry, this model cannot distinguish $O_I$ and $O_{II}$.

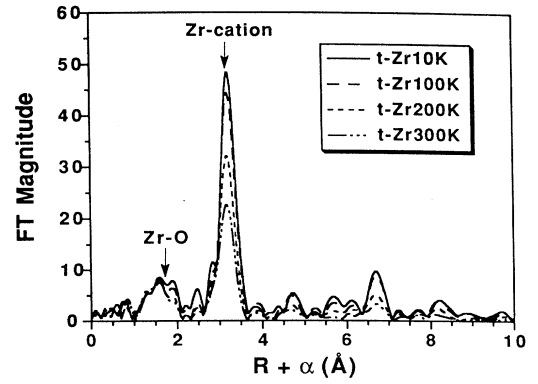


FIG. 3. Temperature dependence of Fourier transform of Zr EXAFS for Y-stabilized $t$-$ZrO_2$.

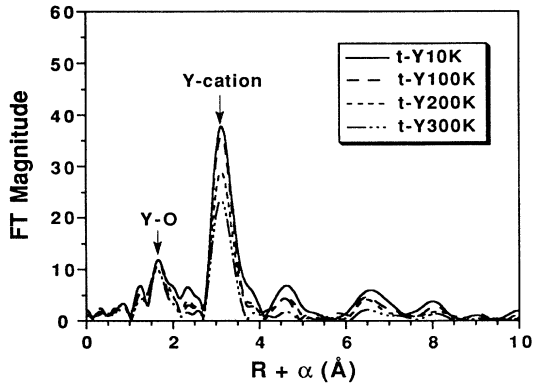


FIG. 5. Temperature dependence of Fourier transform of Y EXAFS for Y-stabilized $t$-$ZrO_2$.

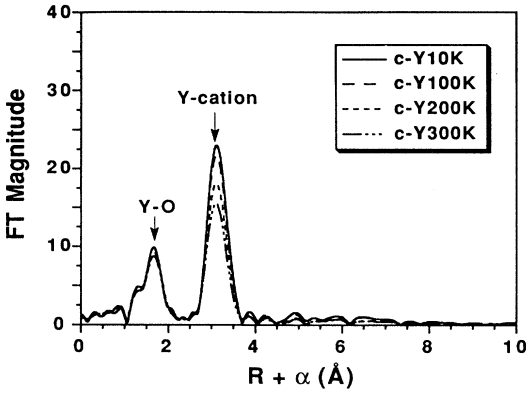


FIG. 6. Temperature dependence of Fourier transform of Y EXAFS for Y-stabilized $c$-$ZrO_2$.

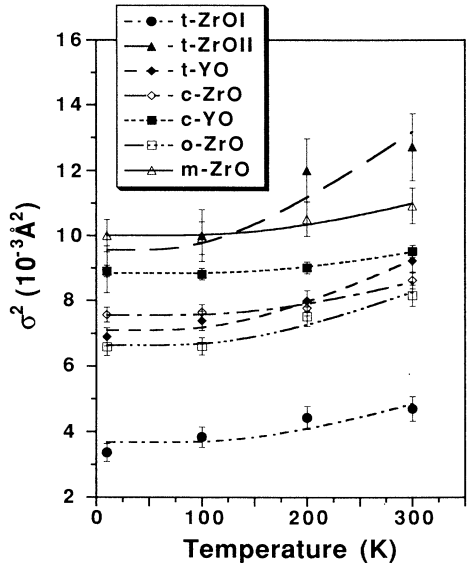


FIG. 7. Comparison of Debye-Waller factor between experimental data (points) and calculated results (lines) for cation-oxygen shell in the four zirconia polymorphs.

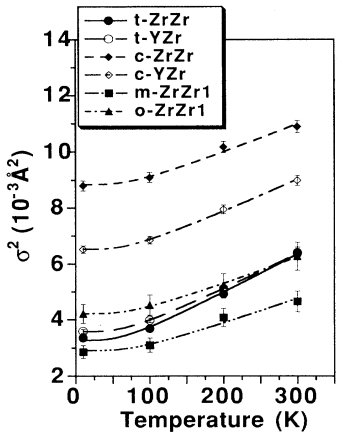


FIG. 8. Comparison of Debye-Waller factor between experimental data (points) and calculated results (lines) for cation-cation shell in the four zirconia polymorphs.

Thus only one set of displacement and dispersion values for oxygen can be deduced from diffraction. This is obviously incomplete in view of our results.

The Y-O bonding has also been investigated, and the results are shown in Fig. 7 and Table I. The Y-O bonding in $t$-$ZrO_2$ is again eightfold, but has a smaller static dispersion (0.0032 Å$^2$) than the Zr-$O_{II}$ shell at the same bond length. This suggests that the Y-O bond is more ordered and probably stronger than the Zr-$O_{II}$ bond. In cubic zirconia, the eightfold-coordinated Y-O shell has a larger static dispersion (0.0062 Å$^2$) than the sevenfold Zr-O shell (0.0045 Å$^2$), probably because of the size misfit of Y (oversized).

#### 2. Cation-cation shells

As described in I, the NNN Zr-Zr scattering in $m$-$ZrO_2$ and $o$-$ZrO_2$ arises from multiple subshells. Only the values for the first subshell are listed in Table I. These values are probably highly correlated to the other subshells and are not discussed further.

Comparing $t$-$ZrO_2$ and $c$-$ZrO_2$, we find that the static dispersion of the Zr-centered cation network (0.0081 Å$^2$) is larger than that of the Y-centered cation network (0.0057 Å$^2$) in cubic zirconia, and both are much larger than the static distortions (0.0023 and 0.0027 Å, respectively) in tetragonal zirconia. In I and II, the large distortion of the Zr cation has been attributed to a noncentrosymmetric displacement of cation along the ⟨111⟩ direction and thought to be responsible for the apparent contraction of Gaussian distance between Zr and cation. We now see that much of this distortion is static in nature.

### C. Thermal distortion

#### 1. Cation-oxygen shells

The frequencies listed in Table I for the cation-oxygen shells are deduced from the Einstein model. The quality of the fit using these frequencies is quite good, as can be seen from Fig. 7. Similar mean vibrational frequencies are obtained for the Zr-O shell in $m$-$ZrO_2$ (410 cm$^{-1}$) and $c$-$ZrO_2$ (406 cm$^{-1}$). Since similar bond lengths and coordination numbers are also obtained, it seems quite certain that the bonding in both phases is similar. In cubic zirconia, the oversized Y dopant adopts eightfold coordination. Despite a longer bond distance, the Y-O shell nevertheless has a higher frequency (461 cm$^{-1}$) than the Zr-O shell. Indeed, this frequency is the highest one of all the cation-oxygen bonds in Table I and probably means the strongest bond. In contrast, the Zr-O shell in $o$-$ZrO_2$ has a lower frequency (350 cm$^{-1}$) despite the same bond length and coordination number as $m$-$ZrO_2$ and $c$-$ZrO_2$. A weaker bond in this metastable phase is thus implied.

The tetragonal phase is also metastable at low temperatures. The fitting results in Table I show a much lower vibrational frequency for the outer Zr-$O_{II}$ bond (266 cm$^{-1}$) than for the inner Zr-$O_I$ bond (389 cm$^{-1}$). Evidently, the outer four oxygen ions are much more weakly

TABLE I. Static distortion and vibration frequency of cation-oxygen and cation-cation shells.

| Composition | Phase | Bonding | R (Å) | $N_{CN}$ | $\sigma^2_{stat}$ (Å$^2$)[a] | $\bar{\nu}$ (cm$^{-1}$)[a] |
|---|---|---|---|---|---|---|
| | | Zr-O | 2.16 | 7.0 | 0.0070 | 410 |
| Pure $ZrO_2$ | *m* | Zr-Zr | 3.46 | 7.0 | 0.0021 | 219 |
| | | | 4.01 | 4.0 | | |
| | | | 4.55 | 1.0 | | |
| | | Zr-O | 2.17 | 7.0 | 0.0031 | 350 |
| Pure $ZrO_2$ | *o* | Zr-Zr | 3.47 | 6.0 | 0.0035 | 210 |
| | | | 3.78 | 4.0 | | |
| | | | 3.93 | 2.0 | | |
| | | Zr-O | 2.15 | 7.0 | 0.0045 | 406 |
| | | Y-O | 2.33 | 8.0 | 0.0062 | 461 |
| 20 mol% $Y_2O_3$-$ZrO_2$ | *c* | Zr-cation | 3.55 | 12.0 | 0.0081 | 205 |
| | | Y-cation | 3.62 | 12.0 | 0.0057 | 192 |
| | | Zr-$O_I$ | 2.10 | 4.0 | 0.0005 | 389 |
| | | Zr-$O_{II}$ | 2.33 | 4.0 | 0.0049 | 266 |
| 3 mol% $Y_2O_3$-$ZrO_2$ | *t* | Y-O | 2.33 | 8.0 | 0.0032 | 318 |
| | | Zr-cation | 3.62 | 12.0 | 0.0023 | 175 |
| | | Y-cation | 3.62 | 12.0 | 0.0027 | 182 |

[a]Einstein model used for cation-oxygen shells and Debye model used for cation-cation shells.

bound. Comparing the Zr-$O_I$ with the Zr-O in *m*-$ZrO_2$ and *c*-$ZrO_2$, we find the former to have a slightly lower vibrational frequency despite its slightly shorter bond length.

The oversized Y dopant has eightfold coordination in an apparently single-shell arrangement in both *t*-$ZrO_2$ and *c*-$ZrO_2$. Despite this similarity, however, the Y-O bond in *t*-$ZrO_2$ has a significantly lower vibrational frequency. This provides another indication of the importance of phase stability in considering bond strength.

### 2. *Cation-cation shells*

The frequencies listed in Table I for the cation-cation shells are deduced from the Debye model. A comparison of the calculated curves and the experimental data is shown in Fig. 8. Except for *t*-$ZrO_2$, the vibrational frequencies for all of the cation-cation bonds are similar in magnitude. These frequencies are lower than the Einstein frequencies of the cation-oxygen diatomic vibrations, pointing to a weaker cation-cation vs cation-oxygen interaction. The frequencies are the lowest for the tetragonal structure. This is responsible for the more rapid decrease in the second peak amplitude for *t*-$ZrO_2$ (Figs. 3 and 5).

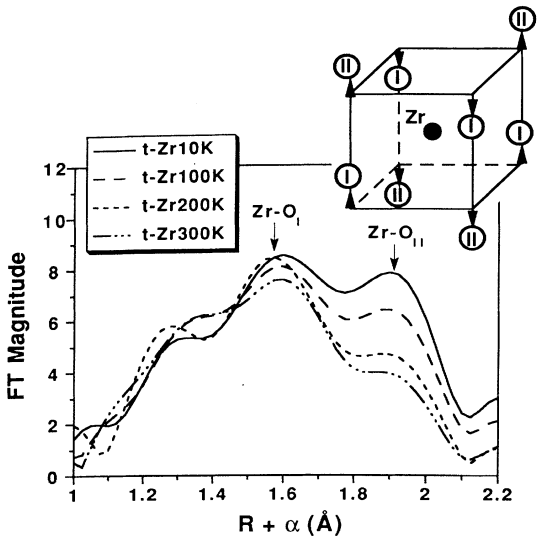


FIG. 9. Temperature dependence of the Fourier transforms for the Zr-O shell in *t*-$ZrO_2$.

## IV. DISCUSSION

### A. Modes of bond distortion in fluorite-related structures

There is a large difference in the static and thermal distortion of the Zr-$O_I$ and Zr-$O_{II}$ subshells in *t*-$ZrO_2$ (Table I). The observation of two frequencies shows that the Zr-$O_I$ and Zr-$O_{II}$ interactions are different even though $O_I$ and $O_{II}$ are crystallographically equivalent in this space group. The local environment of the oxygen may be represented by a distorted tetrahedron, as shown in Fig. 10, with four Zr ions at the corners at two sets of bond distances, Zr-$O_I$ and Zr-$O_{II}$. The fact that $\sigma^2_{stat}$ for Zr-$O_I$ is much smaller than that for Zr-$O_{II}$ indicates that one of the main modes of static distortion is along the $[\pm 1 \pm 10]$ direction. This can be seen from Fig. 10 which shows that the $[\pm 1 \pm 10]$ displacement of the oxygen atom is perpendicular to two of the Zr-O bonds and is at 35° from the other two Zr-O bonds. Thus, if the first two Zr-O bonds are Zr-$O_I$ and the second two are Zr-$O_{II}$, this displacement will give a small $\sigma^2_{stat}$ for Zr-$O_I$ but a large $\sigma^2_{stat}$ for Zr-$O_{II}$. In other words, it stretches and bends the Zr-$O_{II}$ bonds, but only bends the Zr-$O_I$ bonds.

A qualitative assignment of the vibrational modes responsible for the observed $\sigma^2_{vib}$ can now be made by comparison with the Raman spectra. Tetragonal zirconia has six well-defined Raman modes which have been categorized into the following groups[11]

(1) 639 and 609 cm$^{-1}$: Zr-$O_I$ stretching.

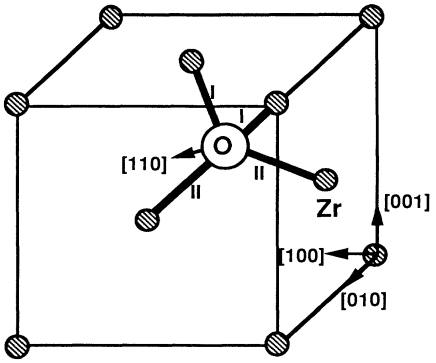


FIG. 10. Oxygen distortion along $[\pm 1 \pm 10]$ direction in $t$-$ZrO_2$

(2) 465 and 321 $cm^{-1}$: coupling of $O_I/O_{II}$-Zr-$O_I/O_{II}$ bending and Zr-$O_I/O_{II}$ stretching.

(3) 259 $cm^{-1}$: mainly Zr-$O_{II}$ stretching.

(4) 147 $cm^{-1}$: $O_I$-Zr-$O_I$ and Zr-$O_I$-Zr bending.

Obviously, the high frequencies of group (1) do not contribute to our data. This implies that these modes are not thermally excited at 300 K. It is also evident that group (3) corresponds to thermal distortion of Zr-$O_{II}$ (266 $cm^{-1}$). The primary vibrational distortion for Zr-$O_I$, which has an apparent Einstein frequency of 389 $cm^{-1}$, is probably a mixture of group (2) vibrations. Referring to Fig. 10, this means that while Zr-$O_I$ is not stretched but mostly bent, the displacement nevertheless couples some Zr-$O_{II}$ stretching and bending.

Analysis of the Zr-cation distortion is more complicated since they cannot be purely acoustic modes; they involve only the cation network, as assumed in the Debye model. They necessarily contain contributions from Zr-O-Zr and even O-Zr-O distortion, and thus have some characteristics of an optical mode. If an Einstein model is used to estimate a vibrational frequency, we obtain a lower value of 134 $cm^{-1}$, compared to 175 $cm^{-1}$ found with the Debye model. These two frequencies bracket the group (4) vibration and suggest that Zr-$O_I$-Zr and $O_I$-Zr-$O_I$ are mainly involved in Zr-Zr vibration.

The less distorted Y-O polyhedron has an environment midway between Zr-$O_I$ and Zr-$O_{II}$. We propose that its principal distortion, seen at an apparent frequency of 318 $cm^{-1}$ in the EXAFS, involves contributions from both groups (2) and (3). The Y-cation distortion again corresponds to group (4), but is slightly stiffer than the Zr-cation distortion because of phase-stability considerations. (See next subsection.)

Turning to $c$-$ZrO_2$, we recall that the local environment of the Zr in $c$-$ZrO_2$ is not fluoritelike; its Zr-O coordination is sevenfold, and its cation lattice is highly distorted because of the difficulty in arranging $ZrO_7$ polyhedra into fcc packing.[4,5] However, Y-O is eightfold coordinated and the local cation network around Y is probably fluoritelike. This picture finds support in the frequency of Y-O distortion at 461 $cm^{-1}$, which is close to the unique Raman mode, 466 $cm^{-1}$, for $T_{2g}$ symmetry of $MO_2$ oxides with fluorite structures ($CeO_2$, $ThO_2$, and $UO_2$).[12] This mode also belongs to group (2). The other frequencies (Zr-O and cation-cation) for $c$-$ZrO_2$ do not seem to reflect the fluorite structure, but are similar to those found in $m$-$ZrO_2$ which, like $c$-$ZrO_2$, is made of $ZrO_7$ polyhedra and is thermodynamically stable.

### B. Phase stability and alloying effect

Comparison of the static and thermal distortions of the cation-oxygen and cation-cation shells for different polymorphs and cations reveals a systematic trend which may be attributed to phase stability and the alloying effect of Y. In general, we expect a less stable phase to have a larger distortion and the Y dopant to have a local stabilizing effect. Among the phases we studied, $t$-$ZrO_2$ is least stable, followed by $o$-$ZrO_2$. $m$-$ZrO_2$ and $c$-$ZrO_2$ are stable phases.[4] A higher frequency is then associated with phase stability or, locally, with a stabilizing dopant.

Our data show that the frequencies of the Zr-O and Zr-Zr distortions in $m$-$ZrO_2$ are higher than those in $o$-$ZrO_2$, despite their structural similarity. This is in accord with their relative phase stability. Similarly, the frequencies of the Zr-cation and Y-cation distortions in the $c$-$ZrO_2$ are higher than those in $t$-$ZrO_2$, despite their similar 12-fold coordination. This can also be rationalized by their relative phase stability. A further example is given by the Y-O frequency, which is higher in $c$-$ZrO_2$ and lower in $t$-$ZrO_2$, despite the fact that the Y-O bond lengths and coordination numbers are the same in both phases. This is again consistent with the relative phase stability. As an example of the stabilizing effect of a dopant, we note that $t$-$ZrO_2$ has a higher frequency for Y-cation distortions than for Zr-cation distortions and that the Y-O distortion has a much higher frequency than Zr-$O_{II}$ distortions, despite the similar bond length. The slightly lower frequency for Y-cation distortion compared to Zr-cation distortion in the cubic phase is somewhat surprising. This may mean that the Zr-cation network in $c$-$ZrO_2$ is locally closer to that in $m$-$ZrO_2$, in view of their similar $ZrO_7$ polyhedra, so that its Debye frequency is also closer to the latter. In contrast, the Y-cation environment is more fluoritelike and thus its frequency is closer to that in tetragonal zirconia.

### C. Comparison with Debye-Waller factors from diffraction studies

For a diatomic compound $AB$, the EXAFS Debye-Waller factor ($\sigma^2_{AB}$) is fundamentally different from the diffraction Debye-Waller factor ($u^2_A$ or $u^2_B$). The former refers to the mean-square *relative* displacements along the direction ($\hat{\mathbf{R}}_{AB}$) between absorbing ($A$) and backscattering ($B$) atom, whereas the latter refers to the mean-square *absolute* displacement of an individual atom ($A$ or $B$) around its equilibrium position. Their relationship can be written as[13]

$$\sigma^2_{AB} = \langle (\hat{\mathbf{R}}_{AB} \cdot \mathbf{u}_A)^2 \rangle + \langle (\hat{\mathbf{R}}_{AB} \cdot \mathbf{u}_B)^2 \rangle - 2\langle (\hat{\mathbf{R}}_{AB} \cdot \mathbf{u}_A)(\hat{\mathbf{R}}_{AB} \cdot \mathbf{u}_B) \rangle \ . \quad (4)$$

The last term is a correlation term which vanishes if the

TABLE II. Comparison of Debye-Waller factor ($10^{-3}$ Å$^2$) between EXAFS and neutron diffraction.

| EXAFS[a] | | | | Diffraction | | | | |
|---|---|---|---|---|---|---|---|---|
| Composition | Phase | Zr-O | Zr-cation | Composition | Phase | Oxygen | Cation | Ref. |
| $(Zr,Y)O_{1.971}$ | $t$ | 4.8 ($O_I$)<br>12.8 ($O_{II}$) | 6.4 | $(Zr,Y)O_{1.968}$ | $t$ | 12.4 | 8.2 | 14 |
| $(Zr,Y)O_{1.834}$ | $c$ | 8.5 | 10.9 | $(Zr,Y)O_{1.87}$ | $c$ | 20.0 | 15.2 | 15 |

[a]Present study.

absorbing atom ($A$) and the scattering atom ($B$) move independently. If $A$ and $B$ move as a rigid body, the last term is negative and will substantially reduce the magnitude of $\sigma^2_{AB}$.

The available diffraction data[14,15] were mostly obtained at room temperature and have not been decomposed into static and thermal contributions. Thus only the total Debye-Waller factors at room temperature are compared. These values are summarized in Table II.

First, we compare the Zr-cation distortion, i.e., $A=$Zr and $B=$Zr or Y. If we assume that Zr and Y both distort in a random manner, then the projection for $A$, $\langle(\hat{\mathbf{R}}_{AB}\cdot\mathbf{u}_A)^2\rangle$, is $u^2_A/3$ and likewise for $B$, and the correlation term vanishes. Since diffraction techniques cannot distinguish Zr from Y, we let $u^2_A=u^2_B$. Thus the EXAFS Debye-Waller factor is predicted to be about $\frac{2}{3}$ of the diffraction Debye-Waller factor. This is in agreement with the data shown in Table II for both the tetragonal and cubic phases. The cation distortion is thus mostly uncorrelated.

We next consider Zr-O distortion. The Zr-$O_I$ distortion in $t$-$ZrO_2$ is highly correlated, as seen by the small value of $\sigma^2_{ZrO_I}$ compared to $u^2_{Zr}$ and $u^2_O$ (Table II). In contrast, $\sigma^2_{ZrO_{II}}$ is much larger and comparable to $u^2_O$. This is possible, for example, if the Zr distortion is nearly random with respect to the Zr-$O_{II}$ bond direction, but the $O_{II}$ distortion is primarily along the Zr-$O_{II}$ bond direction, giving

$$\langle(\hat{R}_{ZrO_{II}}\cdot\mathbf{u}_{Zr})^2\rangle\approx u^2_{Zr}/3\ ,$$

$$\langle(\hat{\mathbf{R}}_{ZrO_{II}}\cdot\mathbf{u}_O)^2\rangle\approx u^2_O\ ,$$

and

$$\langle(\hat{\mathbf{R}}_{ZrO_{II}}\cdot\mathbf{u}_{Zr})(\hat{\mathbf{R}}_{ZrO_{II}}\cdot\mathbf{u}_O)\rangle\approx 0\ .$$

Other possibilities that can similarly explain the above data also exist. (Note that the random, uncorrelated Zr-Zr distortion ($u^2_{Zr}$) already destroys the crystallographic equivalency of $O_I$ and $O_{II}$ locally. Yet diffraction methods still cannot distinguish $O_I$ and $O_{II}$.) Comparison of the magnitude of $\sigma^2_{ZrO}$ with $u^2_{Zr}$ and $u^2_O$ in the cubic phase indicates intermediate correlation of the cation-O distortion. It is interesting to note that the Zr-O bond length in $c$-$ZrO_2$ is also halfway between those for Zr-$O_I$ and Zr-$O_{II}$ in $t$-$ZrO_2$.

In summary, the cation-cation distortion is mostly uncorrelated, while the cation-anion distortion is largely correlated, especially for shorter bonds. This is reasonable considering the lack of direct bonding between cations and the bond-strength–bond-length correspondence for cation-anion bonding.

## V. CONCLUSIONS

(1) Static distortions and vibrational frequencies for the cation-oxygen and the first cation-cation shell in zirconia polymorphs have been quantitatively determined. Interatomic distance, coordination number, and phase stability are found to have an important influence on the observed distortions.

(2) Tetragonal zirconia has two types of Zr-O bonding. Although $O_I$ and $O_{II}$ are crystallographically equivalent in an undistorted lattice, they have essentially different static bond dispersion, vibrational frequency, and correlated motion relative to Zr. The inner oxygen atoms have a smaller distortion, a higher frequency, and a stronger correlation.

(3) The sevenfold Zr-O polyhedra in cubic and monoclinic zirconia have the same vibrational frequency because of similar bonding despite the large difference in crystal symmetry and chemical composition. The vibrational frequency of the eightfold Y-O polyhedron in cubic zirconia is the highest among cation-O bonds in these materials and coincides with the characteristic Raman frequency for prototypical fluorite-type oxides ($CeO_2$, $ThO_2$, and $UO_2$). Similarly bonded Y-O in tetragonal zirconia has a much lower frequency because of phase instability.

(4) The Zr-cation network in tetragonal zirconia has the softest vibrational frequency among all of the polymorphs, reflecting phase instability. Also, compared to (stable) monoclinic zirconia, (metastable) orthorhombic zirconia has lower frequencies for Zr-O and Zr-Zr distortions despite the structural similarity between these polymorphs.

## ACKNOWLEDGMENTS

We are grateful to Dr. Ohtaka (Osaka University) for providing the orthorhombic powder and to Dr. B. Hedman and J. deWitt (both SSRL) for experimental assistance. SSRL is funded by the U.S. Department of Energy with additional support from the U.S. National Institute of Health. This research is supported by the U.S. National Science Foundation under Grant No. DMR-9119598.

[1]B. K. Teo, *EXAFS: Basic Principles and Data Analysis* (Springer-Verlag, New York/Berlin, 1986), pp. 91–102.
[2]C. Y. Yang, M. A. Paesler, and D. E. Sayers, Phys. Rev. B **36**, 980 (1987).
[3]P. P. Lottici and J. J. Rehr, Solid State Commun. **35**, 565 (1980).
[4]P. Li, I-W. Chen, and J. E. Penner-Hahn, this issue, Phys. Rev. B **48**, 10 063 (1993).
[5]P. Li, I-W. Chen, and J. E. Penner-Hahn, preceding paper, Phys. Rev. B **48**, 10 074 (1993).
[6]O. Ohtaka and S. Kume, J. Am. Ceram. Soc. **71**, C-164 (1985).
[7]O. Ohtaka, T. Yamanaka, S. Kume, N. Hara, H. Asano, and F. Izumi, Proc. Jpn. Acad. B **66**, 193 (1990).
[8]J. J. Rehr, J. Mustre de Leon, S. I. Zabinsky, and R. C. Albers, J. Am. Chem. Soc. **113**, 5135 (1990).
[9]E. Sevillano, H. Meuth, and J. J. Rehr, Phys. Rev. B **20**, 4908 (1979).
[10]G. Beni and P. M. Platzman, Phys. Rev. B **14**, 1514 (1976).
[11]D. Michel, M. T. Van Den Borre, and A. Ennaciri, in *Science and Technology of Zirconia III,* edited by S. Somiya, N. Yamamoto, and H. Hanagida, Advances in Ceramics Vol. 24 (The American Ceramic Society, Westerville, OH, 1988), pp. 555–562.
[12]V. G. Keramidas and W. B. White, J. Chem. Phys. **59**, 1561 (1973).
[13]Ref. 1, pp. 62–63.
[14]C. J. Howard, R. J. Hill, and B. E. Reichert, Acta Crystallogr. B **44**, 116 (1988).
[15]D. Steel and B. E. F. Fender, J. Phys. C **7**, 1 (1974).